Math. & Comput. Sci., 6(3) 2025, 49–60

Online: ISSN 2717-2708

Mathematics and Computational Sciences

Journal Homepage: http://mcs.qut.ac.ir/mcs

Extended Luttinger-Tisza analysis of magnetic phases in frustrated honeycomb lattices

Mohammad Hossein Zare[a,*], Hamid Mosadeq[b]

[a]Department of Physics, Qom University of Technology, Qom 37181-46645, Iran

[b]Department of Physics, Faculty of Science, Shahrekord University, Shahrekord 88186-34141, Iran

Abstract

This paper presents a numerical investigation of the classical spin-1/2 Heisenberg $J_1 - J_2$ model on the two-dimensional honeycomb lattice, primarily utilizing eigenvalue-based methods. We employ both the standard and extended versions of the Luttinger-Tisza method to determine classical ground states and phase transitions as a function of the frustration ratio, J_2/J_1. The standard Luttinger-Tisza method, through Fourier transformation and global spin normalization, reduces the Hamiltonian to an eigenvalue problem in momentum space, thereby enabling the identification of Néel and spiral spin liquid phases. In contrast, the Extended Luttinger-Tisza method, implemented in real space, incorporates permutation operators and coupling matrices defined on multi-spin unit cells, thus facilitating the detection of more complex magnetic orders such as zigzag and stripy phases. Our analysis reveals significant discrepancies between the two methods, particularly in the high-frustration regime ($J_2/J_1 > \frac{1}{2}$), highlighting the necessity of symmetry-adapted real-space computations for accurately characterizing frustrated systems. Beyond $J_2/J_1 > \frac{1}{2}$, the extended method computationally delineates the stripy phase. In contrast, the standard method predicts a Néel phase in this regime, which can be attributed to its global spin normalization constraint. These results illustrate the efficacy of such mathematical and numerical techniques in classifying spin model ground states and provide a robust framework for future analytical and computational studies.

Keywords: Runge-Kutta method, Extended Luttinger-Tisza method, Heisenberg model, Honeycomb lattice, Spiral spin liquid.

2020 MSC: 47H10, 54H25

1. Introduction

In the field of quantum magnetism, the spin liquid phase is characterized as a highly entangled state that exhibits a lack of conventional long-range magnetic order even at absolute zero temperature [1, 2, 3]. While quantum spin liquids (QSLs) are distinguished by their exotic characteristics, such as fractionalized excitations and topological order, analogous states known as classical spin liquids can arise in geometrically frustrated systems. In contrast to their quantum counterparts, the degeneracy and magnetic disorder observed in classical spin liquids are attributed to competing interactions and lattice geometry, rather than to quantum fluctuations.

*Corresponding author

Email addresses: zare@qut.ac.ir (Mohammad Hossein Zare), hamid.mosadegh@gmail.com (Hamid Mosadeq)

doi: 10.30511/mcs.2025.2061616.1362

Received: 24 May 2025 Accepted: 13 September 2025

The classical Heisenberg $J_1 - J_2$ model on the honeycomb lattice serves as a prototypical system for investigating frustration-induced magnetic phenomena. In this model, J_1 and J_2 represent the nearest-neighbor and next-nearest-neighbor exchange interactions, respectively. Although the honeycomb lattice is bipartite and unfrustrated for $J_2 = 0$, the introduction of a finite $J_2 > 0$ induces geometric frustration. This frustration can destabilize conventional magnetic orders, such as the Néel antiferromagnetic phase, leading to the emergence of disordered or noncollinear magnetic phases characterized by extensive degeneracy in momentum space [4, 5].

A particularly intriguing regime in frustrated spin systems arises when the level of frustration is sufficiently strong to preclude a unique ground state while remaining inadequate to establish conventional long-range magnetic order. In the classical Heisenberg $J_1 - J_2$ model on the honeycomb lattice, for example, a classical spiral spin liquid phase is observed when $J_2/J_1 > 1/6$ [4, 5]. This phase is characterized by a ground-state energy that exhibits degeneracy along a continuous contour in momentum space, typically centered around high-symmetry points within the Brillouin zone. Such extensive degeneracy serves as a hallmark of classical spin liquid behavior.

From a rigorous mathematical perspective, the underlying problem necessitates a comprehensive analysis of the spectral characteristics of structured interaction matrices, particularly under various symmetry constraints. This methodology provides significant insights into the principles of eigenvalue optimization within the framework of physically realized lattice structures.

The Luttinger-Tisza method is a well-established analytical technique commonly utilized to ascertain the classical ground state of Heisenberg-type models [6, 7]. This method simplifies the problem by relaxing the local constraint of fixed spin length at individual lattice sites, instead imposing a global constraint. Consequently, the problem is transformed into an eigenvalue analysis of the Fourier-transformed interaction matrix. While the conventional Luttinger-Tisza method is effective in identifying regions of degeneracy and potential ground states, it demonstrates limitations in characterizing phases with complex unit cells or subtle symmetry breaking. To address these limitations, advanced techniques that incorporate permutation symmetries and real-space spin structuressuch as the Extended Luttinger-Tisza methodbecome essential [8].

The extended Luttinger-Tisza method offers a comprehensive framework for the analysis of spin Hamiltonians by constructing these models in real space and incorporating lattice symmetries through the application of permutation operators on spin components within a magnetic unit cell. This methodology facilitates the investigation of intricate spin configurations, including zigzag, stripy, and other commensurate collinear orders, by permitting the expansion of the magnetic unit cell size and the development of corresponding interaction matrices. A significant advantage of the extended Luttinger-Tisza method lies in its capacity to differentiate between various symmetry-broken phases, as it is not limited to translationally invariant solutions within momentum space.

Recent developments highlight the complementary roles of numerical and machine learning methodologies in the investigation of frustrated quantum systems. For instance, Xu et al. successfully classified quantum phases through the application of neural network techniques, yielding insights that extend beyond those provided by conventional analytical methods [9]. Similarly, Liu et al. utilized tensor network simulations to elucidate ground-state properties and emergent orders within frustrated lattice models [10]. Although our approach is predominantly analytical, the integration of these diverse perspectives fosters a more comprehensive understanding of the field and underscores the broader significance of our findings.

In this study, we conduct a systematic investigation of the classical phase diagram for the Heisenberg $J_1 - J_2$ model on the honeycomb lattice. Our analysis utilizes both the standard Luttinger-Tisza method and the extended Luttinger-Tisza method. The primary objectives of this research are to accurately delineate phase boundaries, identify potential ground states, and explore the emergence of classical spin liquid phases as a function of the frustration ratio J_2/J_1.

The remainder of this paper is organized as follows. We commence by introducing the classical Heisenberg $J_1 - J_2$ model on the honeycomb lattice and delineating the theoretical methodologies employed. An analysis of the classical phase diagram is subsequently conducted utilizing the standard Luttinger-Tisza

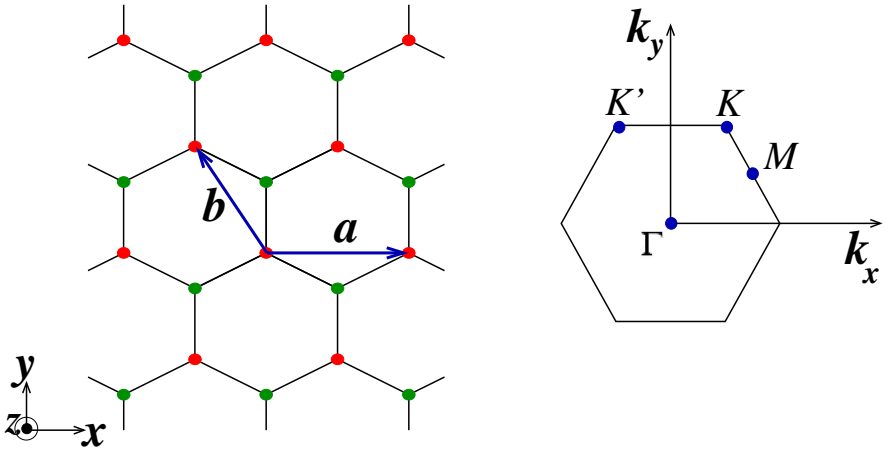

Figure 1: Real-space representation of the two-dimensional honeycomb lattice is presented. The lattice is characterized by two basis vectors, **a** and **b**, which define the unit cell. (b) The corresponding first Brillouin zone of the honeycomb lattice in reciprocal space is depicted, emphasizing the significant high-symmetry points (Γ, K, M, K').

method, with particular emphasis on the emergence of Néel and spiral spin liquid phases as a function of the J_2/J_1 coupling ratio. Following this, we employ the extended Luttinger-Tisza method to examine the stability of various magnetic orders, including zigzag and stripy configurations, by constructing appropriate magnetic unit cells and analyzing their corresponding coupling matrices. A comparative discussion of the results derived from both analytical approaches ensues, highlighting the pivotal role of magnetic frustration and symmetry in determining the ground state. Finally, the paper concludes with a summary of our principal findings and a succinct discussion on prospective future research directions, particularly in relation to quantum effects and potential experimental realizations.

2. Heisenberg Model

This study examines the classical phase diagram on the spin-$\frac{1}{2}$ $J_1 - J_2$ honeycomb Heisenberg model, characterized by the Hamiltonian:

$$\mathcal{H} = \sum_{\langle ij \rangle} J_1 \mathbf{S}_i \cdot \mathbf{S}_j + \sum_{\langle\langle ij \rangle\rangle} J_2 \mathbf{S}_i \cdot \mathbf{S}_j \tag{2.1}$$

In this context, the notations $\langle ij \rangle$ and $\langle\langle ij \rangle\rangle$ represent summations over all nearest-neighbor (NN) and next nearest-neighbor (NNN) bonds, respectively.

3. Method and Results

3.1. Luttinger-Tisza Method

To ascertain the classical phase diagram of the generic model Hamiltonian delineated in Eq. (2.1), we initiate our analysis by utilizing the Luttinger-Tisza approximation. This approach mitigates the stringent fixed spin length constraint imposed at each site by employing a more lenient condition:

$$\sum_i |S_i|^2 = N \tag{3.1}$$

In this context, N represent the total number of lattice points. By employing a Fourier transform on Eq. (2.1) and subsequently diagonalizing the resultant matrix, it is possible to ascertain the stable magnetic configurations as a function of the constant coupling parameters. This process will be discussed in greater detail in the following.

The honeycomb lattice, characterized by a basis of two sites per unit cell ($\nu \in 1,2$), can be decomposed into two interpenetrating triangular Bravais sublattices. These sublattices are generated by the primitive translational vectors ($\mathbf{a} = \hat{x}$) and ($\mathbf{b} = -\frac{1}{2}\hat{x} + \frac{\sqrt{3}}{2}\hat{y}$) [as depicted in Fig. 1(a)]. The Fourier transforms of the spin operators defined on each sublattice (ν) are expressed as follows:

$$S^{\nu}_{\rho}(\mathbf{r}_i) = \frac{1}{\sqrt{N/2}} \sum_{\mathbf{k}} S^{\nu}_{\mathbf{k},\rho} e^{-i\mathbf{k}\cdot\mathbf{r}_i}, \tag{3.2}$$

In this context, $\rho \in x, y, z$ denotes the x, y, or z component of the spin, while $N/2$ represents the system size as measured by the number of primitive unit cells. The summation over the wavevector k is performed within the first Brillouin zone (FBZ) [Fig. 1(b)]. Rewriting the spin Hamiltonian (Eq. 2.1) in terms of the Fourier components of the spin operators, $S^{\nu}_{\mathbf{k},\rho}$, leads to:

$$\mathcal{H} = \sum_{\mathbf{k}} \sum_{\alpha,\beta\in\{\nu\}} \tilde{S}^{\alpha T}_{-\mathbf{k}} H^{\alpha\beta}_{\mathbf{k}} \tilde{S}^{\beta}_{\mathbf{k}} \tag{3.3}$$

where $\tilde{S}^{\alpha}_{\mathbf{k}} = \begin{pmatrix} S^{\alpha}_{\mathbf{k},x} & S^{\alpha}_{\mathbf{k},y} & S^{\alpha}_{\mathbf{k},z} \end{pmatrix}^{T}$. Moreover, the 6×6 matrix $H^{\alpha\beta}_{\mathbf{k}}$, whose elements are the Fourier transforms of the exchange interactions. By transforming to the orthonormal basis constituted by the six normalized eigenmodes of $H_{\mathbf{k}}$ (which forms a 6×6 unitary matrix), Eq. (3.3) is expressed in the form:

$$\mathcal{H} = \sum_{\mathbf{k}} \sum_{\mu=1}^{6} \lambda^{\mu}_{\mathbf{k}} |\mathbf{S}^{'\mu}_{\mathbf{k}}|^2 \tag{3.4}$$

In this context, $\lambda^{\mu}_{\mathbf{k}}$ denotes the μ-th eigenvalue of $H_{\mathbf{k}}$, and the associated eigenvector $w^{\mu}_{\mathbf{k}}$ satisfies the following relation:

$$H_{\mathbf{k}} w^{\mu}_{\mathbf{k}} = \lambda^{\mu}_{\mathbf{k}} w^{\mu}_{\mathbf{k}} \tag{3.5}$$

Furthermore, $\mathbf{S}^{'\mu}_{\mathbf{k}}$ is referred to as the spin structure factor, defined by the expression

$$\mathbf{S}^{'\mu}_{\mathbf{k}} = w^{\mu}_{\mathbf{k}} \tilde{\mathbf{S}}_{\mathbf{k}} \tag{3.6}$$

In this approach, to derive the spin configurations corresponding to the set of coupling constants in Eq. (2.1), it is imperative to identify a global minimum λ_0. By imposing a weak constrain in momentum space, the classical energy, as expressed in Eq. (3.4), can be reformulated as:

$$\mathcal{H} = N\lambda_0 + \sum_{\mathbf{k}} \sum_{\mu\neq 0} (\lambda^{\mu}_{\mathbf{k}} - \lambda_0) |\mathbf{S}^{'\mu}_{\mathbf{k}}|^2 \tag{3.7}$$

Minimizing the classical energy necessitates that the second term in Eq. (3.7) equals to zero due to $(\lambda^{\mu}_{\mathbf{k}} - \lambda_0) > 0$ for $\mu > 0$. This condition requires the elimination of the spin structure factor coefficients $\mathbf{S}^{'\mu}_{\mathbf{k}}$ for $\mu \neq 0$, thereby facilitating the identification of potential ground state spin configurations. For the sake of simplicity, we set $J_1 = 1$.

To ascertain the zero-temperature phase diagram of the spin model delineated in Eq. (2.1) as a function of J_2, we utilize the Runge-Kutta method to minimize λ_0, which signifies the ground state energy. The minimization of the lowest eigenvalue (λ_0) is accomplished through the application of the Runge-Kutta method across discrete momentum vectors within the Brillouin zone. This method enables the accurate identification of phase transition points. Our numerical analysis identifies three distinct phases within the spin-$\frac{1}{2}$ $J_1 - J_2$ model: (i) A commensurate Neél-type antiferromagnetic (AFM) state occurring for $J_2 < 1/6$. (ii) A classical spiral (SP) spin liquid phase for $J_2 > 1/6$. This phase is characterized by a significant ground-state degeneracy, allowing the wave vector to assume any value along contours in momentum space, which are centered around the Γ point and the vertices K and K' of the first Brillouin zone (FBZ), as illustrated in Fig. 2. Notably, for $1/6 < J_2 < 1/2$, these contours are concentrated around the Γ point, whereas for $J_2 > 1/2$, they are localized around the K and K' points.

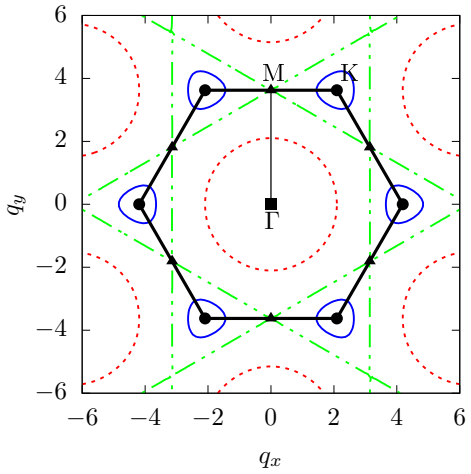

Figure 2: Momentum-space degeneracy of spin spirals is illustrated for varying values of J_2. The black hexagonal boundary denotes the first Brillouin zone. Comparison of contours for varying J_2 values. The red dashed-dot line denotes $J_2 = 0.25$, the green dotted line indicates $J_2 = 0.5$, and the blue solid line represents $J_2 = 0.75$.

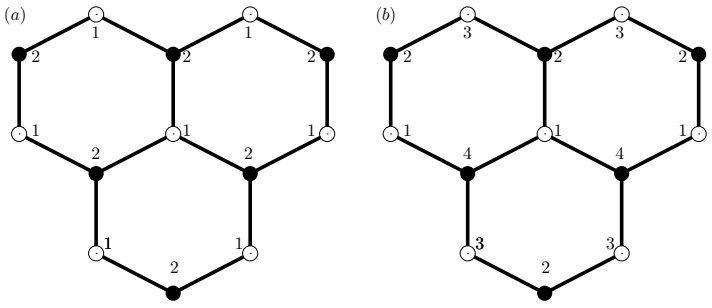

Figure 3: (a) Honeycomb lattice with a two-spin unit cell, (b) honeycomb lattice with a four-spin unit cell.

3.2. Extended Luttinger-Tisza Method

Within this method, the identification of the system's magnetic states requires the preliminary derivation of the coupling matrix $\mathcal{A}_{ij}^{\alpha\beta}$, which is defined as follows:

$$\mathcal{A}_{ij}^{\alpha\beta} = \sum_{l\in\{j\}} \mathcal{J}_{il}^{\alpha\beta} \tag{3.8}$$

In this context, the summation over l includes all neighboring spins that interact with the spin at site i. As an illustrative example, consider the first-neighbor Heisenberg model defined on a honeycomb lattice characterized by a two-site unit cell [Fig. 3(a)]. In this framework, the S^x component of the spin at site 1 within the unit cell engages in interaction with the S^x component of the spin at site 2, yielding a matrix element denoted as $\mathcal{A}_{12}^{xx} = 3J_1$. Analogous considerations pertain to the y and z spin components. Consequently, the coupling matrix $\mathcal{A}$ for the nearest-neighbor Heisenberg model on a honeycomb lattice can be articulated as:

$$\mathcal{A} = \begin{pmatrix} 0 & 0 & 0 & 3J_1 & 0 & 0 \\ 0 & 0 & 0 & 0 & 3J_1 & 0 \\ 0 & 0 & 0 & 0 & 0 & 3J_1 \\ 3J_1 & 0 & 0 & 0 & 0 & 0 \\ 0 & 3J_1 & 0 & 0 & 0 & 0 \\ 0 & 0 & 3J_1 & 0 & 0 & 0 \end{pmatrix} \tag{3.9}$$

The matrix representation of $\mathcal{A}$ can also be expressed as:

$$\hat{\mathcal{A}} = \sum_{i,j} \sum_{\alpha,\beta} \chi_i^{\alpha} \mathcal{A}_{ij}^{\alpha,\beta} \chi_j^{\beta} \tag{3.10}$$

in which the indices of the first summation (i, j) represents the positions within a unit cell, while the indices of the second summation (α, β) designates the spin components. The eigenvector χ_i^{α} associated with the eigenvalue λ of $\hat{\mathcal{A}}$ satisfies the following relation:

$$\sum_{\beta,j} \mathcal{A}_{ij}^{\alpha,\beta} \chi_j^{\beta} = \lambda \chi_i^{\alpha} \tag{3.11}$$

In the extended Luttinger-Tisza method, it is imperative to define a set of permutation operators that corresponds in number to the spins within the unit cell. The application of these operators to two distinct sites results in the interchange of the spins located at those sites. Importantly, the unit cell for various magnetic orders may encompass one, two, or multiple spins. For example, in the case of antiferromagnetic order on a honeycomb lattice, the unit cell consists of two spins that are oriented antiparallel to one another. The two-site permutation operator is defined as follows:

$$P_1 = I, \qquad P_2 = (1, 2) \tag{3.12}$$

These operators possess two eigenvectors, which can be expressed as follows:

$$q(1) = \begin{pmatrix} 1 \\ 1 \end{pmatrix}, \qquad q(2) = \begin{pmatrix} -1 \\ 1 \end{pmatrix} \tag{3.13}$$

The ferromagnetic order is distinctly represented by the eigenvector $q(1)$, which is characterized by its invariance under the two-spin permutation operator. Conversely, the eigenvector $q(2)$, which exhibits a sign change upon permutation, is associated with the antiferromagnetic order.

To enhance clarity and conciseness, the eigenvalues corresponding to the specified eigenvectors are presented in Table 1:

	P_1	P_2
$q(1)$	1	1
$q(2)$	1	-1

Table 1: Eigenvalues for the two-site permutation operator

Given the commutative property of the permutation operators, these operators possess a complete set of simultaneous eigenvectors, thereby facilitating the determination of their corresponding eigenvalues. The application of the permutation operator P_t to the eigenvector $q(t)$ results in the interchange of the elements at positions i and j. This transformation can be mathematically represented as:

$$(P_t q)_j = q_i \tag{3.14}$$

Consequently, the identification of the eigenvalues and eigenvectors requires the resolution of the following characteristic equation:

$$P_t q(k) = \epsilon_t(k)\mathbf{q}(k) \tag{3.15}$$

Given the symmetry $\mathcal{A}^{\alpha\beta}_{P_t i, P_t j} = \mathcal{A}^{\alpha\beta}_{i,j}$, the eigenvector χ^{α}_i can be expressed as:

$$\chi^{\alpha}_i = q_i(t)\phi^{\alpha}(l) \tag{3.16}$$

Substituting Eq. (3.16) into Eq. (3.11) results in:

$$\sum_{\beta,j} \mathcal{A}^{\alpha,\beta}_{ij} q_j(k)\phi^{\beta}(l) = \lambda^l_k \phi^{\alpha}(l) \tag{3.17}$$

According to the definition of the permutation operator:

$$\left[P_{(i,j)} q(k)\right]_j = \epsilon_{P_{(i,j)}}(k) q_j(k) = q_i(k) \tag{3.18}$$

Eq. (3.17) can be rewritten as:

$$\sum_{\beta,j} \mathcal{A}^{\alpha,\beta}_{ij} \epsilon_{P_{(i,j)}} \phi^{\beta}(l) = \lambda^l_k \phi^{\alpha}(l) \tag{3.19}$$

By defining $\mathcal{L}^{\alpha,\beta}_k = \sum_j \mathcal{A}^{\alpha,\beta}_{ij} \epsilon_{P_{(i,j)}}$, Eq. (3.19) can be reexpressed as:

$$\mathcal{L}_k \phi(l) = \lambda^l_k \phi(l) \tag{3.20}$$

Consequently, the i-th component of the spin at the j-th position is described by the following equation:

$$\chi^{\alpha}_i = q_i(k)\phi^k_{\alpha}(l) \tag{3.21}$$

This real-space reformulation results in an eigenvalue problem characterized by matrices that inherently preserve permutation symmetries. This property facilitates the identification of magnetic phases as representations of eigenmodes that maintain invariance under these permutations.

For the purpose of clarity, we commence our analysis with the first-neighbor Heisenberg model on a honeycomb lattice, postulating a magnetic order cell comprising two spins. The matrices $\mathcal{L}_k$ associated with the first-neighbor Heisenberg interaction on the honeycomb lattice are obtained as follows:

$$\mathcal{L}_1 = \begin{pmatrix} 3J_1 & 0 & 0 \\ 0 & 3J_1 & 0 \\ 0 & 0 & 3J_1 \end{pmatrix}, \quad \mathcal{L}_2 = \begin{pmatrix} -3J_1 & 0 & 0 \\ 0 & -3J_1 & 0 \\ 0 & 0 & -3J_1 \end{pmatrix} \tag{3.22}$$

This analysis demonstrates that the matrix $\mathcal{L}_2$ exhibits a lowest eigenvalue that is degenerate for all three spin components. This degeneracy suggests an antiparallel alignment of the spin components of the two

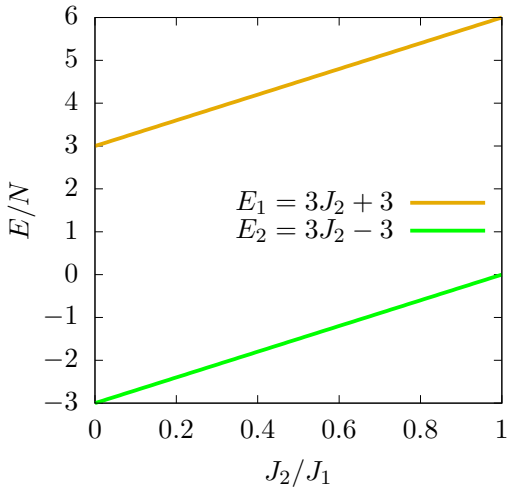

Figure 4: Dependence of the eigenvalues of the $\mathcal{L}_{1,2}$ matrix on the J_2/J_1 ratio in the Heisenberg $J_1 - J_2$ model on the honeycomb lattice. These findings correspond to calculations conducted within two-spin unit cells, with J_1 fixed at unity.

spins within a unit cell, thereby indicating the stability of the Neél order for the fist-neighbor Heisenberg model on the honeycomb lattice.

For the two-spin unit cell of the honeycomb lattice, the coupling matrix $\mathcal{A}$ associated with the first- and second-neighbor Heisenberg Hamiltonian is defined as follows:

$$\mathcal{A} = \begin{pmatrix} 3J_2 & 0 & 0 & 3J_1 & 0 & 0 \\ 0 & 3J_2 & 0 & 0 & 3J_1 & 0 \\ 0 & 0 & 3J_2 & 0 & 0 & 3J_1 \\ 3J_1 & 0 & 0 & 3J_2 & 0 & 0 \\ 0 & 3J_1 & 0 & 0 & 3J_2 & 0 \\ 0 & 0 & 3J_1 & 0 & 0 & 3J_2 \end{pmatrix} \tag{3.23}$$

The matrices $\mathcal{L}_k$ associated with the various eigenvalues are given by:

$$\mathcal{L}_1 = \begin{pmatrix} 3J_1 + 3J_2 & 0 & 0 \\ 0 & 3J_1 + 3J_2 & 0 \\ 0 & 0 & 3J_1 + 3J_2 \end{pmatrix}, \quad \mathcal{L}_2 = \begin{pmatrix} -3J_1 + 3J_2 & 0 & 0 \\ 0 & -3J_1 + 3J_2 & 0 \\ 0 & 0 & -3J_1 + 3J_2 \end{pmatrix} \tag{3.24}$$

Extending the analysis of the nearest-neighbor Heisenberg model on the honeycomb lattice, we find that the magnetic order remains stable despite the introduction of a second-neighbor Heisenberg interaction (J_2), particularly when examining the two-spin unit cell configuration. As demonstrated in Eq. (3.24), the eigenvalues of $\mathcal{L}_{1,2}$ are degenerate across all three spin components. Simultaneously, the $\mathcal{L}_2$ eigenvalue displays the lowest value within the range of J_2 values investigated, as illustrated in Fig. 4.

As previously discussed, the extended Luttinger-Tisza method offers a comprehensive framework for the analysis of magnetic order stability. This method involves the construction of magnetic unit cells to represent distinct, potentially stable magnetic configurations on the honeycomb lattice. By comparing the relative energies of these unit cells, one can ascertain the stability of a particular magnetic order as a function of J_2. To examine the stability of specific phases, such as zigzag and stripy, a four-spin magnetic cell is employed [Fig. 3](b).

Since the calculation of $\mathcal{L}_k^{\alpha,\beta}$ is independent of i, the matrix $\mathcal{A}_{i,j}^{\alpha,\beta}$ is examined solely for $i = 1$:

$$\mathcal{A}_{i=1,j} = \begin{pmatrix} J_2 & 0 & 0 & 2J_1 & 0 & 0 & 2J_2 & 0 & 0 & J_1 & 0 & 0 \\ 0 & J_2 & 0 & 0 & 2J_1 & 0 & 0 & 2J_2 & 0 & 0 & J_1 & 0 \\ 0 & 0 & J_2 & 0 & 0 & 2J_1 & 0 & 0 & 2J_2 & 0 & 0 & J_1 \end{pmatrix} \tag{3.25}$$

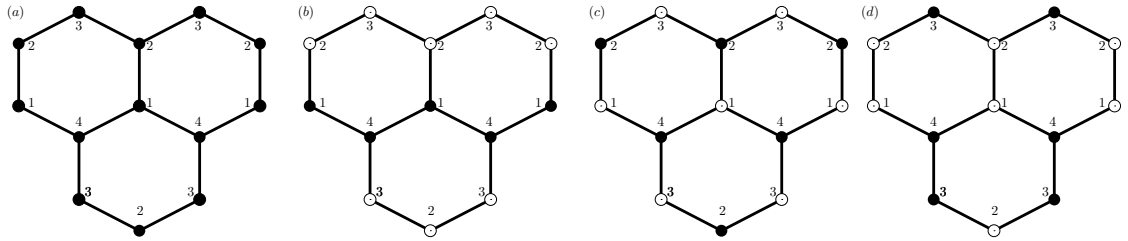

Figure 5: Illustrative spin configurations for various magnetic orders on the honeycomb lattice, within a four-site unit cell, (a) Ferromagnetic phase, associated with eigenvector $q(1)$, exhibiting complete spin polarization. (b) Zigzag order, depicted by eigenvector $q(2)$, (c) Néel antiferromagnetic order, corresponding to eigenvector $q(3)$, and (d) Stripy order, characterized by eigenvector $q(4)$.

Given magnetic orders characterized by a four-site unit cell, the corresponding four-spin permutation operators are delineated as follows:

$$\begin{aligned} P_1 &= I, & P_2 &= (12)(34), \\ P_3 &= (13)(24), & P_4 &= (14)(23) \end{aligned} \tag{3.26}$$

Similar to the two-spin unit cell, it is feasible to compute the eigenvalues and eigenvectors for this case. Eigenvectors associated with these permutation operators are given by:

$$q(1) = \begin{pmatrix} +1 \\ +1 \\ +1 \\ +1 \end{pmatrix}, \quad q(2) = \begin{pmatrix} +1 \\ -1 \\ -1 \\ +1 \end{pmatrix}, \quad q(3) = \begin{pmatrix} -1 \\ +1 \\ -1 \\ +1 \end{pmatrix}, \quad q(4) = \begin{pmatrix} -1 \\ -1 \\ +1 \\ +1 \end{pmatrix} \tag{3.27}$$

The ferromagnetic order is distinctly characterized by the eigenvector $q(1)$, which is notable for its invariance under the two-spin permutation operator, as depicted in [Fig. 5(a)]. In contrast, eigenvector $q(3)$, which demonstrates a sign change upon permutation, is representative of the antiferromagnetic order [Fig. 5(c)]. The zigzag magnetic order is exemplified by eigenvector $q(2)$, as illustrated in Fig. 5(b), while the stripy magnetic order is also associated with eigenvector $q(2)$, as presented in Fig. 5(d).

To enhance clarity and conciseness, the eigenvalues corresponding to the specified eigenvectors are presented in Table 2.

	P_1	P_2	P_3	P_4
$q(1)$	+1	+1	+1	+1
$q(2)$	+1	-1	-1	+1
$q(3)$	+1	-1	+1	-1
$q(4)$	+1	+1	-1	-1

Table 2: Eigenvalues for the four-site permutation operator.

For this case, the matrices $\mathcal{L}_k$ associated with the various eigenvalues are given by:

$$\mathcal{L}_1 = \begin{pmatrix} 3J_1+3J_2 & 0 & 0 \\ 0 & 3J_1+3J_2 & 0 \\ 0 & 0 & 3J_1+3J_2 \end{pmatrix}, \quad \mathcal{L}_2 = \begin{pmatrix} -J_1-J_2 & 0 & 0 \\ 0 & -J_1-J_2 & 0 \\ 0 & 0 & -J_1-J_2 \end{pmatrix},$$

$$\mathcal{L}_3 = \begin{pmatrix} -3J_1+3J_2 & 0 & 0 \\ 0 & -3J_1+3J_2 & 0 \\ 0 & 0 & -3J_1+3J_2 \end{pmatrix}, \quad \mathcal{L}_4 = \begin{pmatrix} J_1-J_2 & 0 & 0 \\ 0 & J_1-J_2 & 0 \\ 0 & 0 & J_1-J_2 \end{pmatrix} \tag{3.28}$$

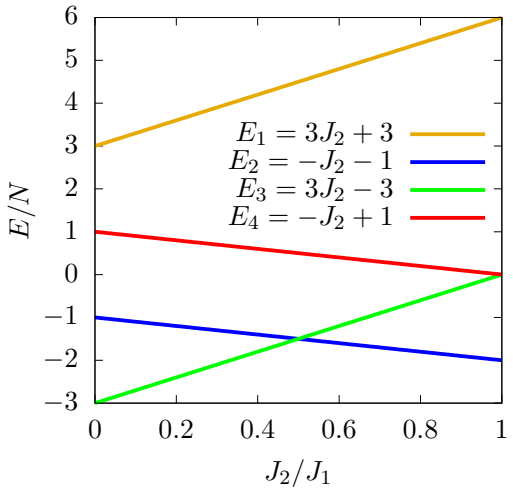

Figure 6: Dependence of the eigenvalues of the $\mathcal{L}_{1,\ldots,4}$ matrix on the J_2/J_1 ratio in the Heisenberg $J_1 - J_2$ model on the honeycomb lattice. These findings correspond to calculations conducted within four-spin unit cells, with J_1 fixed at unity.

To examine the stability of different magnetic phases, the eigenvalues of the $\mathcal{L}_k$ matrices are plotted as a function of J_2, as illustrated in Fig. 6. For each value of J_2, the spin arrangement associated with the lowest eigenvalue is identified. This analysis is conducted specifically for the case where $J_2 > 0$.

As illustrated in Fig. 6, the eigenvalue of the $\mathcal{L}_3$ matrix, specifically $-3J_1 + 3J_2$, indicates the lowest energy state for the condition $J_2 < \frac{1}{2}$. To ascertain the corresponding spin configuration, Eq. (3.21) is employed. Accordingly, the projection of the spins within the four-spin unit cell along the x-direction is expressed as follows:

$$\chi^{\alpha=x} = q(3) \begin{pmatrix} +1 \\ 0 \\ 0 \end{pmatrix} = \begin{pmatrix} -1 & +1 & -1 & +1 \end{pmatrix} \begin{pmatrix} +1 \\ 0 \\ 0 \end{pmatrix} = \begin{pmatrix} -1 \\ 0 \\ 0 \\ +1 \\ 0 \\ 0 \\ -1 \\ 0 \\ 0 \\ +1 \\ 0 \\ 0 \end{pmatrix} \tag{3.29}$$

To further validate the spin configuration, calculations were performed for the y and z directions. The results were consistent with those from the x direction, thereby confirming an alternating antiparallel spin arrangement within the four-spin unit cell. This confirms that for $J_2 < \frac{1}{2}$, the magnetic order is the Néel order.

For $J_2 > \frac{1}{2}$, the eigenvalue of the $\mathcal{L}_2$ matrix, given by $-J_1 - J_2$, corresponds to the lowest energy state. In this case, the spin projections within the four-spin unit cell are oriented in various directions, as

determined by the eigenvector

$$\chi^{\alpha=x} = q(2)\begin{pmatrix}+1\\0\\0\end{pmatrix} = \begin{pmatrix}+1 & -1 & -1 & +1\end{pmatrix}\begin{pmatrix}+1\\0\\0\end{pmatrix} = \begin{pmatrix}+1\\0\\0\\-1\\0\\0\\-1\\0\\0\\+1\\0\\0\end{pmatrix} \tag{3.30}$$

To further validate the spin configuration, calculations were performed for the y and z directions. The results were consistent with those from the x direction, thereby confirming an antiparallel spin arrangement within the four-spin unit cell, as depicted in Fig. 5(c) This spin configuration corresponds to the stripy magnetic order. Our results, however, diverge from those obtained by the Luttinger-Tisza method: while the extended Luttinger-Tisza method predicts the stripy order to be stable for $J_2 > \frac{1}{2}$, the stable order identified by the Luttinger-Tisza method is the Néel order.

4. Conclusion

In this study, we conducted a numerical investigation of the classical phase diagram of the spin-1/2 Heisenberg $J_1 - J_2$ model on the honeycomb lattice employing both the standard and Extended Luttinger-Tisza methods. The standard approach, which relies on momentum-space eigenvalue minimization, successfully identified Néel and spiral spin liquid phases through an analysis of Brillouin zone degeneracy. In contrast, the extended method reformulates the eigenvalue problem in real space by utilizing permutation symmetries and expanded unit cells, allowing for a more accurate identification of complex magnetic orders, including zigzag and stripy phases.

Our findings underscore the significance of real-space numerical methods that explicitly account for lattice symmetries, particularly in highly frustrated regimes where ground states exhibit extensive degeneracy. The observed discrepancies between the predictions of the two methods for $J_2 > \frac{1}{2}$ highlight the limitations inherent in traditional momentum-space techniques and emphasize the necessity for refined numerical frameworks in the examination of frustrated magnetic systems. These results not only enhance our understanding of classical frustrated spin models but also lay a solid foundation for future research into quantum extensions, algorithmic advancements, and the exploration of broader lattice geometries.
The current findings underscore the importance of matrix spectral analysis and the characterization of permutation-invariant eigenspaces as essential components in the accurate delineation of magnetic phase diagrams.

References

[1] Balents, Leon. (2010). Spin liquids in frustrated magnets. Nature, 464(7286), 199-208. 1
[2] Savary, Lucile, Balents, Leon. (2016). Quantum spin liquids: a review. Reports on Progress in Physics, 80(1), 016502. 1
[3] Knolle, Johannes, A Moessner, Roderich. (2019). A field guide to spin liquids. Annual Review of Condensed Matter Physics, 10(1), 451-472. 1
[4] Mulder, A., A Ganesh, R., A Capriotti, L., A Paramekanti, A., (2010). Spiral order by disorder and lattice nematic order in a frustrated Heisenberg antiferromagnet on the honeycomb lattice. Physical Review B, 81(21), 214419. 1
[5] Zare, Mohammad H, Fazileh, Farhad, Shahbazi, Farhad. (2013). Zero-temperature phase diagram of the classical Kane-Mele-Heisenberg model. Physical Review B, 87(22), 224416. 1

[6] Luttinger, JM., A Tisza, L., (1946). Theory of dipole interaction in crystals. Physical Review, 70(11), 954. 1
[7] Litvin, Daniel Bernard, (1974). The luttinger-tisza method. Physica, 77(2), 205. 1
[8] Niemeyer, Th., (1972). On the ground state of crystals with dipole-dipole and exchange interactions. Physica, 57(2), 281-293. 1
[9] Xu, Qichen and Miranda, Ivan P and Pereiro, Manuel and Rybakov, Filipp N and Thonig, Danny and others, (2023). Metaheuristic conditional neural network for harvesting skyrmionic metastable states. Phys. Rev. Research 5(4), 043199. 1
[10] Liu, Wen-Yuan and Poilblanc, Didier and Gong, Shou-Shu and Chen, Wei-Qiang and Gu, Zheng-Cheng., (2024). Tensor network study of the spin- square-lattice model: Incommensurate spiral order, mixed valence-bond solids, and multicritical points. Physical Review B 109(23), 235116. 1